Supporting Information

Probing the mechanical properties of magnetosome chains in living magnetotactic bacteria

André Körnig[1], Jiajia Dong[2,3], Mathieu Bennet[1], Marc Widdrat[1], Janet Andert[1], Frank D. Müller[4], Dirk Schüler[4], Stefan Klumpp[2], and Damien Faivre[1]

[1]Department of Biomaterials, and

[2]Department of Theory and Bio-Systems, Max Planck Institute of Colloids and Interfaces, Science Park Golm, 14424 Potsdam, Germany

[3] Department of Physics and Astronomy, Bucknell University, Lewisburg, PA 17837, USA

[4] Department 1, Microbiology, Ludwig-Maximilians-Universität München, Großhaderner Strasse 2-4, 82152 Planegg-Martinsried, Germany

Corresponding author's email address: damien.faivre@mpikg.mpg.de.

Supporting figures

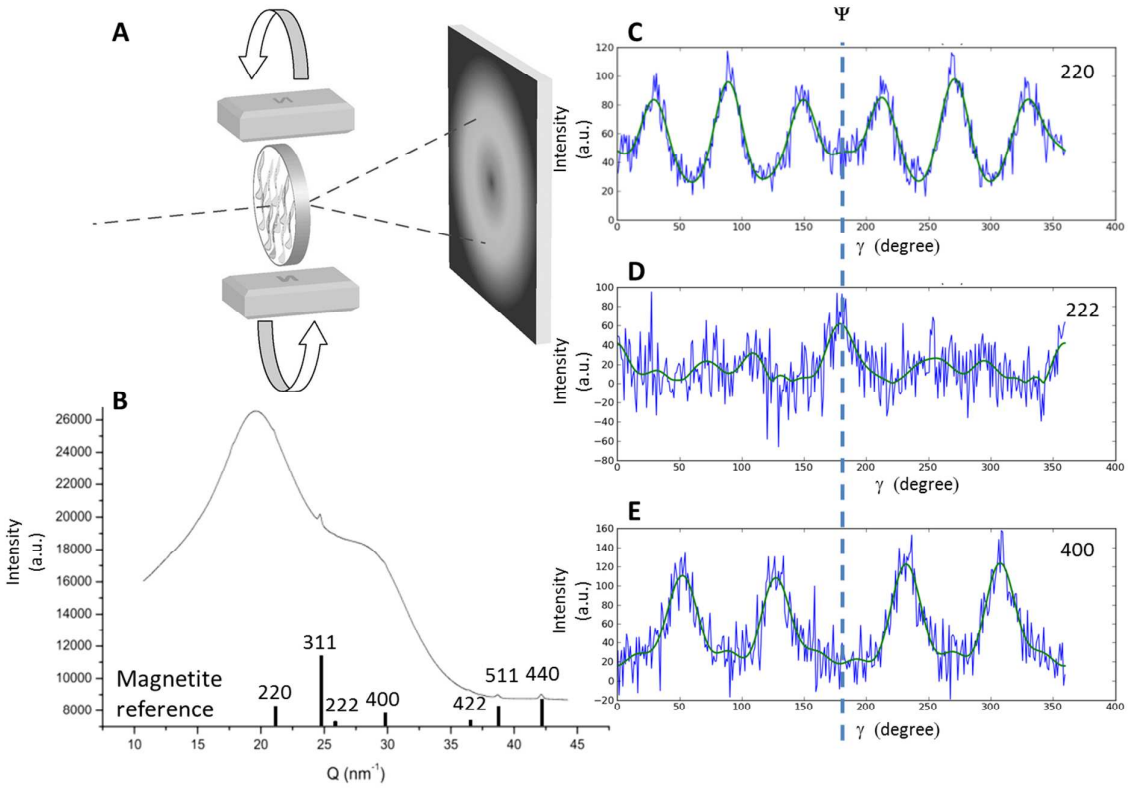

Figure S1: Schematic representation of the XRD experiments with applied magnetic fields and corresponding 2D pattern (A). Resulting azimuthal (B) and radial (C-E) integration of the 2D diffraction patterns. Despite the high amorphous background of the agarose, magnetite is detectable in the diffractogram (B). After local background subtraction, the Debye rings of different planes show azimuthal intensity variations and the angle of the fiber axis can be obtained (C-E). The fiber axis Ψ is added on the graphs for easier visualization.

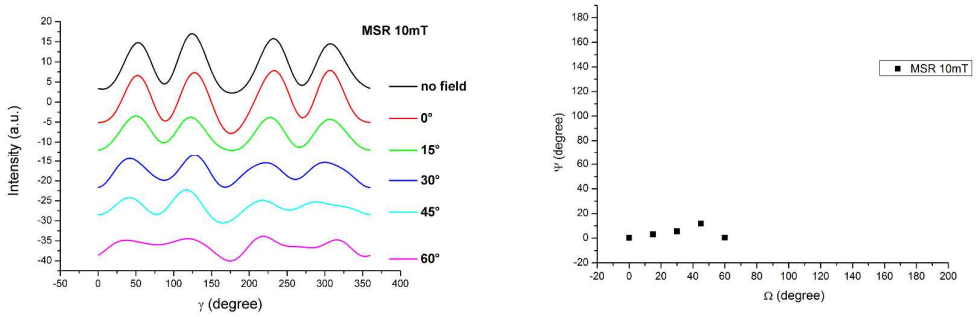

Figure S2: Example of the reduction of texture quality by rotation of weak external fields. The quality of the texture changes with the variation of the direction of the external field. The initially strong azimuthal intensity variations become smaller until they vanish at an angle of 60°. There, the Debye ring shows very little azimuthal intensity variations, and the evaluation of a preferred orientation of the magnetite crystals within the cell is not possible. This effect can be explained by a rotation of some crystals up to higher angles, whereas other crystals stay at low angles. This leads to the loss of a preferred orientation of the majority of the crystals and therefore to no detectable texture.

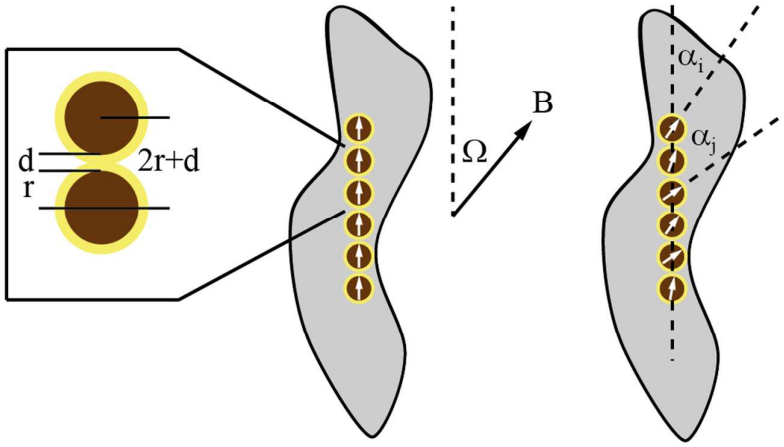

Figure S3: scheme of the parameters used for the theoretical model. *r* is the radius of the particles, *d* the edge to edge distance between two consecutive magnetosomes. The angle *Ω* denotes the angle between the applied magnetic field and the orientation at which the cells were fixed. Finally, the different α are the angles from which the single magnetosome orient towards the external applied field.

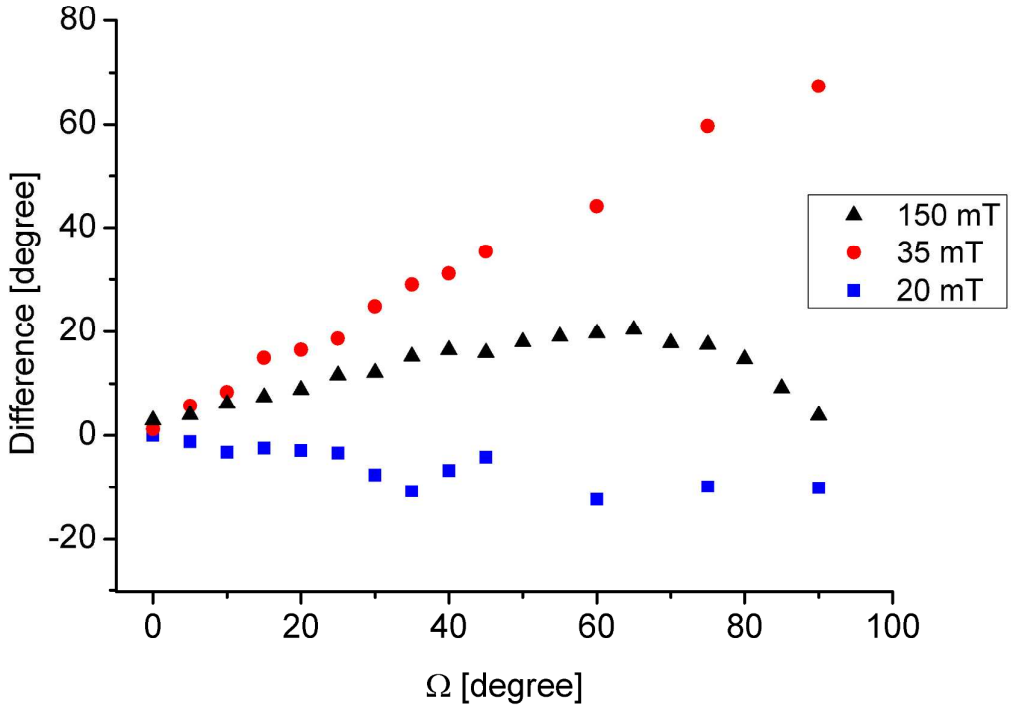

Figure S4: difference between measured and computed angles as a function of the orientation of the external magnetic field Ω.

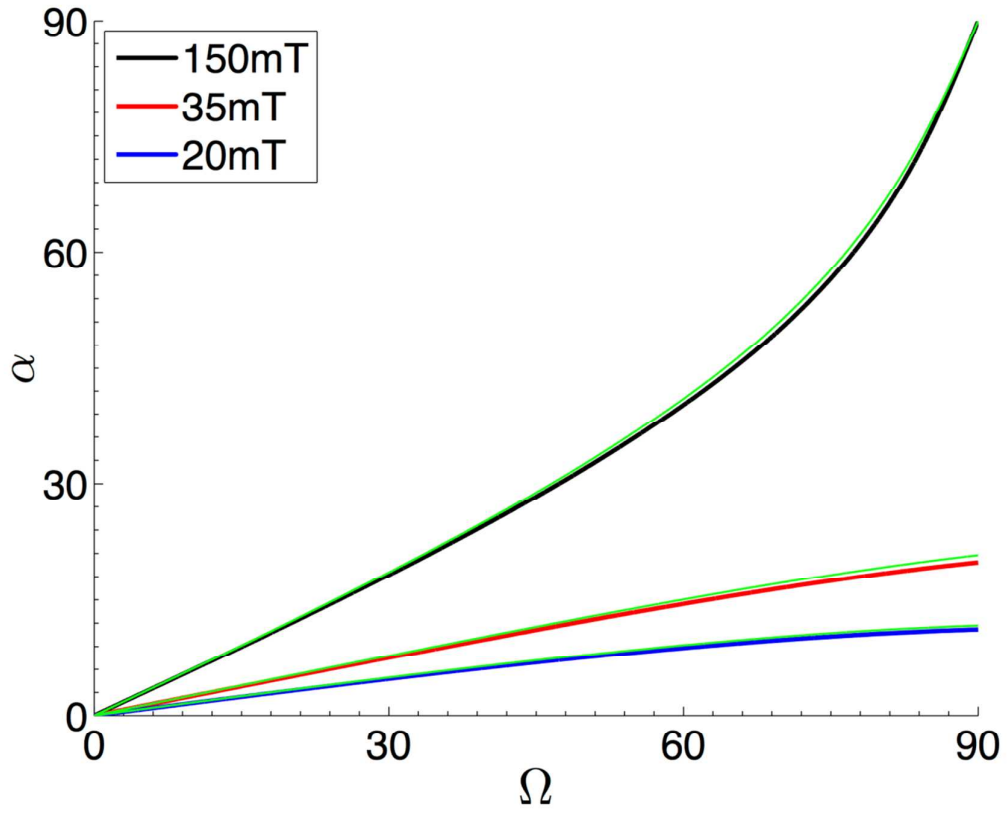

Figure S5: Calculated orientation α of dipoles as a function of the orientation Ω of an external field for a chain of 20 dipoles with r = 20 nm (solid lines) and for a chain with 10 dipoles with r = 20 nm in the center of the chain and 5 dipoles with radius 15 nm at each chain end (thin green lines); d = 10 nm for all magnetosomes.

Theoretical model

In the model, the magnetosome chain is described as a chain of freely rotating interacting magnetic dipoles (discussed below). The energy of the chain consists of two contributions, the interaction of the dipoles with the external magnetic field (E_{ext}) and the dipole-dipole interactions (or the interaction of each dipole with the field generated by all other dipoles, E_{int}).

The external field contribution to the energy can be written as

$$E_{ext} = -\sum_{i=1}^{N} \boldsymbol{m_i} \cdot \boldsymbol{B_{ext}} = -\sum_{\boldsymbol{i=1}}^{\boldsymbol{N}} m_{\boldsymbol{i}} \cdot B_{ext} \cdot \cos(\Omega - \alpha_i) \approx -NnB_{ext} \cos(\Omega - \alpha)$$

(supplementary equation 1)

Here m_i is the magnetic moment of magnetosome *i*, α_i is its angle with respect to the chain axis. $\boldsymbol{B}_{\text{ext}}$ is the external field, B_{ext} its absolute value, and Ω is the angle between the external field and the chain axis. In the last step, we have assumed that all dipoles align with the same angle ($\alpha_i \approx \alpha$ for all *i*). Monte Carlo simulations using the exact expressions show that for chains of 10 or more dipoles, this assumption is very accurate with the exception of the two terminal dipoles, which were seen to deviate by up to 15°. These deviations can be attributed to the fact that these dipoles have only one nearest neighbor, since the dominant contribution to the interaction energy is from the nearest-neighbor interactions.

The internal part of the energy is obtained as a sum over all dipole-dipole interactions,

$$E_{int} = \frac{\mu_0}{4\pi} \sum_{i=1}^{N} \sum_{j=1}^{i-1} \left(\frac{3(\boldsymbol{m}_i \boldsymbol{r}_{ij})(\boldsymbol{m}_j \boldsymbol{r}_{ij})}{r_{ij}^5} - \frac{\boldsymbol{m}_i \cdot \boldsymbol{m}_j}{r_{ij}^3} \right). \qquad \text{(SE2)}$$

The latter expression can be simplified to

$$E_{int} = -\frac{\mu_0}{4\pi} \sum_{i=1}^{N} \sum_{j=1}^{i-1} \frac{m_i m_j}{r_{ij}^3} \left(3 \cos \alpha_i \cos \alpha_j - \cos(\alpha_i - \alpha_j) \right) \quad \text{(SE3)}$$

or, assuming again that all dipoles are characterized by the magnetic moment *m* and the same angle α, to

$$E_{int} \approx -NmB_{int}(3 \cos^2 \alpha - 1). \qquad \text{(SE4)}$$

Here we have defined a characteristic internal field strength B_{int} by

$$B_{int} = \frac{\mu_0}{4\pi} \frac{S_N}{N} \frac{m}{r^3 \left(1 + {}^{d}/_{2r}\right)^3} = \frac{B_0}{\left(1 + {}^{d}/_{2r}\right)^3}, \quad \text{(SE5)}$$

where S_N is related to the generalized harmonic numbers ($H_{n,\alpha} = \sum_{k=1}^{n} k^{-\alpha}$) via $S_N = NH_{N,3} - H_{N,2} \approx 1.2N$; r is the radius of the magnetosomes and *d* is the separating distance between two neighboring magnetosomes (thus 2*r*+*d* is the center-to-center distance

between nearest neighbor magnetosomes). $B_0 \approx 30$ mT is a material parameter independent of the geometric parameters (m/r^3 is the magnetization, i.e. the density of the magnetic moment), which characterizes the maximal internal field strength (obtained for d=0). Minimizing the total energy with respect to the angle α leads to the condition

$$6B_{int}(\cos\alpha \sin\alpha) = B_{ext}\sin(\Omega - \alpha), \qquad \text{(SE6)}$$

from which α is determined numerically.

The description of a magnetosome chain as a chain of magnetic dipoles is a simplification with respect to several aspects of the chains:

(i) Treating magnetosomes as magnetic point dipoles is exact for spherical magnetosomes and provides a good approximation, which is based on the dominant part of the magnetic interactions, for particles of other shapes. For example, for a chain of cubic particles with the same overall magnetization, the energy differs from the dipole approximation only by around 10 % (S. Klumpp et al., manuscript submitted).

(ii) By assuming that the positions of the magnetosomes remain fixed, we neglect their mobility around these positions (which is restricted by the magnetic interactions as well as the link to the cytoskeletal structure). The range of this mobility is however small, as can be estaimated by consindering the energy cost of a displacement. Taking into account only the magnetic interactions with the neighbor particles, the energy of a lateral displacement ε (perpendicular to the chain) leads to an increase in energy of:

$$\Delta E = -\frac{2\mu_0 m^2}{4\pi\,(2r+d)^3}\left[3\cos^5\vartheta - \cos^3\vartheta - 2\right] \text{ with } \vartheta = \tan^{-1}\frac{\epsilon}{2r+d}. \qquad \text{(SE7)}$$

Comparison of this energy (assuming magnetosome particles with r = 20 nm, and d = 10 nm) with the thermal energy, kT ($\approx$ 4 pN nm), leads to a typical lateral displacement of 2 nm or

only 4 % of the center-to center distance of the neighboring magnetosomes. We note that this is an overestimate as it only includes magnetic nearest-neighbor interactions.

(iii) Another simplification in the model is that all magnetosomes have the same size and thus the same magnetic moment, while in a cell, the magnetosome sizes may be heterogeneous, typically with older, larger magnetosomes in the center of the chain and smaller new magnetosomes at the chain's ends. We tested the impact of different sizes by considering chains of 10 magentosomes with r = 20 nm in the center and 5 magnetosomes with r = 15 nm at both ends (note that this difference in radius corresponds to a 2.4-fold difference in volume and thus in magnetization). Results shown in Fig. S5 indicate that the rotation of a magnetic field has almost the same effect for these heterogeneous chains as for the regular chains, but the heterogeneous chains are slightly more aligned with with the external field.

Full Methods

Bacteria growth

Magnetospirillum gryphiswaldense MSR-1 (DSMZ 6361) and the mutants *ΔmamJ* and *mCherry-MamK* were grown in rubber sealed tubes in MSR-1 standard media[37]. The cultures were incubated at 28° C at 100 rpm shaking for 24 h under microaerobic conditions. Bacterial growth and the average magnetic orientation of the cells (C_{mag})[38] were determined by optical measurements at 565 nm (Shimadzu UV-1201V spectrophotometer). For all the samples the OD was around 0.3 and the C_{mag} 0.7 – 0.9.

Immobilization of bacteria

0.1g Low-Melt Agarose (6351, Carl Roth) was dissolved in 10 mL Millipore water resulting in 1 % (w/w) concentration. The solution was heated to 80 °C and swirled until complete dissolution of the agarose. The solution was cooled down slowly to 30 °C, keeping the agarose solution in its liquid state. The bacteria-agarose solution stayed liquid when kept above the gelling temperature of 30 °C. Cooling the solution below the gelling temperature led to crosslinking of the Agarose and a fixation of the bacteria. For the experiments the gel had to be prevented from dehydration, thus a poly-(dimethylsiloxane) PDMS/glass sample holder was built. Briefly, a poly-(methyl methacrylate) PMMA master was fabricated by milling 4 x 4 mm square holes with a depth of 400 µm using a computer numerical control (CNC) milling machine. The surface of the resulting positive pattern in the PMMA substrate was polished in order to remove defects that later would inhibit the binding to a coverslip. A negative PDMS master was produced by replica molding of the PMMA substrate using the Sylgard 184 Silicon Elastomer Kit (Dow Corning). The prepolymer base and the curing agent were mixed in a 10:1 (w/w) ratio and degassed under vacuum to remove air bubbles. The mixture was poured onto the PMMA master and cured for 2h at 70 °C. After curing the PDMS negative master was peeled off the PMMA and treated with 0.1 % (w/w) hydroxypropylmethylcellulose HPMC (Sigma) in PBS. From this negative PDMS master, the sample holders were produced by a second replication. A degassed 10:1 mixture of prepolymer base and curing agent was poured onto the negative PDMS master and cured for 1h at 70 °C. Once cured the PDMS mold is peeled off carefully from the PDMS master. A 10 x 10 mm glass coverslip and the PDMS mold were placed in a plasma cleaner (Harrick Plasma). Immediately after the oxygen containing plasma treatment the PDMS surface was brought

into contact with the coverslip and aged for 1 h at 70 °C. Finally a hole was punched into the PDMS providing the possibility to attach the sample holder by screws to the XRD setup. Two needles were used to inject the bacteria-agarose solution into the PDMS sample holder, where one of the needles was used as an air outlet. The sample holder was placed between two permanent magnets, applying a field of 150 mT. After injection the setup was still kept above 30 °C for at least 15 min, allowing the bacteria to align in the agarose. After that the setup was cooled down slowly to room temperature, and then to 4 °C, where it was stored for at least 15 min. The agarose gelled and the aligned bacteria were fixed in the agarose matrix.

TEM measurements

For TEM analysis the glass was removed from the PDMS and the gel was covered with a 4 % Paraformaldehyde solution with and without a present magnetic field perpendicular to the direction of the bacteria alignment. The Paraformaldehyde conserved the state of the bacteria. After washing the sample with MiliQ water a small amount was transferred to a copper grid with an amorphous carbon support film and let to dry. Transmission electron micrographs were acquired on a Zeiss EM Omega 912 at an acceleration voltage of 120 kV.

XRD

Xray diffraction measurements were performed at the µ-spot beamline at the BESSY II synchrotron radiation facility (Helmholtz-Zentrum Berlin (HZB), Germany) with a 100 µm beam of 15 keV. Two dimensional diffraction patterns were collected using a MarMosaic 225 charge-coupled device-(CCD) based area detector(Mar USA, Evanston, USA).

A motorized rotational set-up was custom-built for the XRD experiments at the Bessy synchrotron. This provided the support for coils (for a magnetic field up to 35 mT) or a pair of permanent magnets (field strength above 100 mT), that were used to generate a magnetic field perpendicular to the beam path The PDMS-glass sample holder was mounted on a brass bar parallel to the beam. This allowed a free rotation of the magnetic field around the sample and perpendicular to the incoming beam, without special restrictions (figure s3).

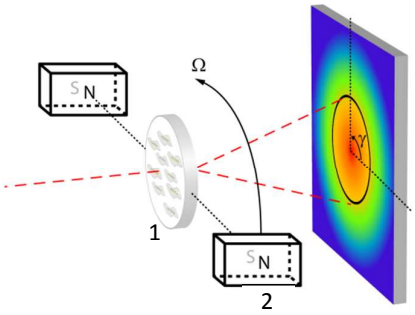

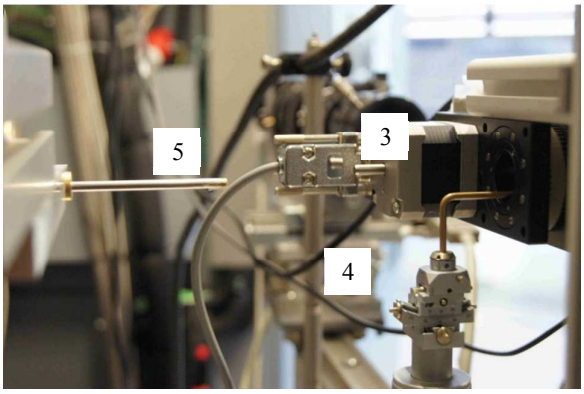

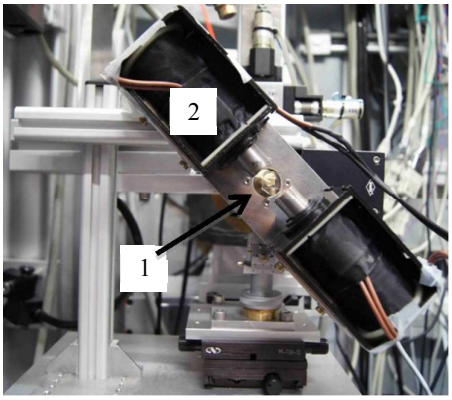

Figure S6: Schematic representation (A) and photographs (B, C) of the custom-made rotation setup for XRD synchrotron measurements. A motorized rotation stage (3) rotates magnets or coils (2) around the sample of mounted in a PDMS/glass sample holder (1) and fixed on a messing bar (4). The pinhole for the beam is fixed on another bar (5) in order to be close to the sample.

Data processing

The analysis of the XRD data was performed using the programs Fit2D (Hammersley, 1997) and Autofit (developed by Cheng Hao Li, Aurien Gourrier and Gerald A. Zickler) as well as several home written python based codes. The combination of these programs allowed batch processing.

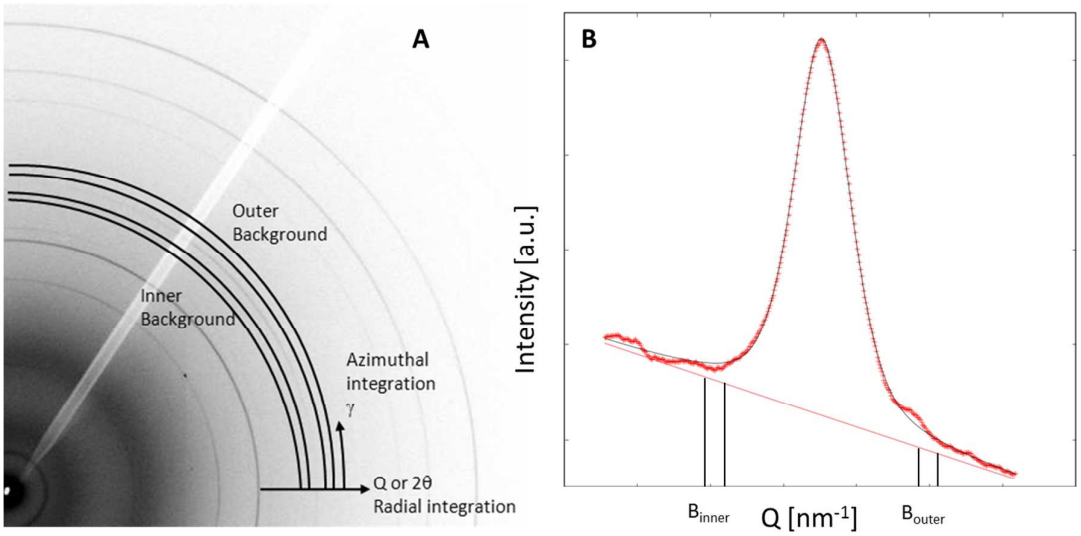

Figure S7: Local background subtraction: Scheme on the 2D pattern (A). The azimuthal integration (thick red line) and peakfit (thin black and thin red line) for evaluation of the Q range for the ring, the inner and the outer background (B).

To gain the intensity variations within the Debye rings a background correction had to be performed, since there are intensity deviations coming from the measurement setup (e.g. beamstop). Figure S6 shows the schematic azimuthal integration and background subtraction. To get the azimuthal intensity distribution $I(\gamma)$ 3 azimuthal integrations were performed for the inner background, the outer background and the ring itself, respectively. The azimuthal intensity variation of the Debye ring is then:

$$I(\gamma) = I_{ring}(\gamma) - \left[B_{outer}(\gamma) - \frac{B_{outer}(\gamma) - B_{inner}(\gamma)}{2}\right]$$

Author Contributions:

D.F., A.K., S.K. and D.S. designed research. A.K. carried out XRD experiments and data analysis. J.D. and S.K. designed the theoretical framework of the work. M.B. performed fluorescence microscopy. M.W. performed electron microscopy. F.D.M. performed the genetic work associated with the generation of fluorescent MamK mutant. J.A. cultured bacteria. D.F. supervised the work and wrote with S.K. the first draft of the manuscript that was commented by all the authors.